Partial Discharge Inception Voltage of Voids Enclosed in Epoxy/Mica versus Voltage Frequency and Temperature

Torstein Grav Aakre and **Erling Ildstad**
Norwegian University of Technology and Science (NTNU)
Department of Electric Power Engineering
NO-7491 Trondheim, Norway

Sverre Hvidsten
SINTEF Energy Research
Department of Electric Power Technology
NO-7465 Trondheim, Norway

ABSTRACT

Detection of partial discharges (PDs) is widely used as a condition assessment tool for high voltage equipment. Application of low frequency test voltage is often preferred in the case of test objects with a large capacitance. The question addressed here is how results from PD-measurements performed at low frequencies correspond to that occurring at 50 Hz power frequency. Different theoretical models for void voltage were examined and compared to experiments performed on laboratory samples of mica/epoxy, including embedded cylindrical voids. All test objects were preconditioned at 10 kV and 50 Hz for 5 min before partial discharge inception voltage (PDIV) testing by stepwise increasing the test voltage from 0 to 10 kV. The PDIV test was first completed at 300 Hz before being repeated at decreasing frequencies down to 0.1 Hz. The temperature was varied in the range of 20° to 155°C. The results at high frequencies showed that a pure capacitive model fits well to the measurements. Measured dielectric response in mica/epoxy explained the decreasing PDIV at low frequencies and high temperatures. A high PDIV was measured at a combination of low temperatures and low frequencies. This was correlated with a reduced void resistance of the electrically stressed void sidewalls caused by the PD activity during the preconditioning period. This indicates that the effect of PD by-products decays faster at higher temperatures. Values of PDIV are, therefore, expected to be dependent on both temperature and frequency.

Index Terms — **partial discharges, rotating machine insulation, cavities, variable frequency**

1 INTRODUCTION

ELECTRICAL condition assessment of high voltage equipment is today performed at different voltage frequencies. It is advantageous to test high voltage equipment with a large capacitance, e.g. generators and cables, by energising them at a very low frequency (VLF) voltage, because these voltage sources are much smaller and easier to apply than the required transformer or resonant source at power frequency. Power frequency tests have been in focus in condition assessment standards [1, 2]. VLF tests can be used, but at a higher voltage [3], and VLF and power frequency tests can give significantly different results.

Several studies have tried to explain partial discharges (PDs) in small voids as a function of frequency. The simplest approach was by using an RC circuit to model an insulation system with a void [4]. They varied the time constants of the insulation and the void. A greater cavity time constant than the material time constant resulted in a higher PD repetition rate at low frequencies. The PD repetition rate decreased when the time constant of the void was smaller than that of the insulation. Other works have compared finite element method (FEM) modelling of various void dimensions of different level of detail to experimental results [5-10], with parameters such as apparent charge and repetition rate vs voltage frequency.

The purpose of this study is to establish an equivalent circuit that can be used to describe the frequency- and temperature-dependent void voltage. This was studied experimentally in a laboratory setup using mica/epoxy samples with an enclosed cylindrical void. This work will discuss the experimental validity of different theoretical models and the mechanisms responsible for frequency-dependent partial discharge inception voltage (PDIV) behaviour at different temperatures.

Manuscript received on 01 July 2019, in final form 20 August 2019, accepted 21 August 2019. Corresponding author: T. G. Aakre.

2 VOID VOLTAGE MODELS

The voltage across a void encapsulated in a dielectric can be modelled by representing the system by an equivalent circuit. To establish such circuits, the void is denoted with subscript c, the series insulation subscript b, and the surrounding insulation parallel subscript a. Edge effects are not included, and the electric field is assumed to be homogeneous in all parts of the insulation.

The first model considered here (Model 1, Figure 1a) is the capacitive so-called abc-circuit equivalent [11], referring to the circuit components as pure capacitances. In the case of modelling PD inception at DC or low voltage frequency, the abc-model is expanded by introducing resistance (Model 2, Figure 1b) and dielectric response (Model 3, Figure 1c) in the insulation. The void resistance R_c consists of both resistance in air and resistance at the surface between sections a and c.

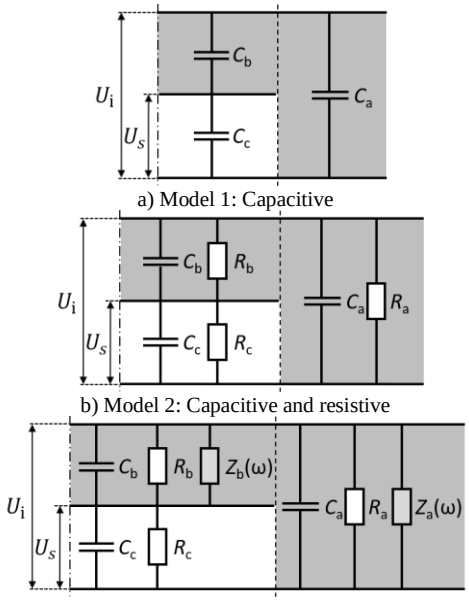

a) Model 1: Capacitive

b) Model 2: Capacitive and resistive

c) Model 3: Capacitive, resistive and dielectric response

Figure 1. Equivalent circuits of an insulation system with a cylindrical void. The insulation is shaded gray, whereas the void is white.

The resulting relations between the applied voltage U_i and the voltage occurring across the void U_s are presented in Equations (1), (2), and (3), assuming a cylindrical void. The definitions of the symbols used in these equations are given in Table 1. The circuit elements are expressed by material parameters to make the equations independent of void area.

Table 1. Definition of parameters used in the models.

Parameter	Definition
U_s	Breakdown voltage in void, based on Paschen curve
U_i	Measured Partial Discharge Inception Voltage for given U_s
d_b	Insulation thickness
d_c	Void gap distance
ω	Angular frequency; $\omega = 2\pi f$, where f is frequency
ε_0	Vacuum permittivity
$\varepsilon_{\mathrm{r,c}}$	Relative permittivity of air
$\varepsilon_{\mathrm{r,b}}$	Relative permittivity of insulation
ε_b^*	Complex permittivity of the insulation
σ_b	Conductivity of the insulation
σ_c	Conductivity of the air in the void

PDIV U_i for given void voltage U_s with Model 1:

$$U_\mathrm{i} = \left(1 + \frac{d_\mathrm{b}}{d_\mathrm{c}} \cdot \frac{\varepsilon_{\mathrm{r,c}}}{\varepsilon_{\mathrm{r,b}}}\right) \cdot U_\mathrm{s}. \qquad (1)$$

PDIV U_i for given void voltage U_s with Model 2:

$$U_\mathrm{i} = \left(1 + \frac{d_\mathrm{b}}{d_\mathrm{c}} \frac{\sigma_c + j\omega\varepsilon_0\varepsilon_{\mathrm{r,c}}}{\sigma_b + j\omega\varepsilon_0\varepsilon_{\mathrm{r,b}}}\right) \cdot U_\mathrm{s}. \qquad (2)$$

PDIV U_i for given void voltage U_s with Model 3:

$$U_\mathrm{i} = \left(1 + \frac{d_\mathrm{b}}{d_\mathrm{c}} \frac{\sigma_\mathrm{c} + j\omega\varepsilon_0\varepsilon_{\mathrm{r,c}}}{\sigma_\mathrm{b} - \frac{\mathrm{Im}\{\varepsilon_\mathrm{b}^*\}}{\omega} + j\omega\mathrm{Re}\{\varepsilon_\mathrm{b}^*\}}\right) \cdot U_\mathrm{s}. \qquad (3)$$

Partial discharge modelling assumes that a discharge occurs when the voltage across the void exceeds the withstand strength of the void. In the case of a homogeneous electric field in the void, the withstand strength of the void given by the Paschen law can be approximated to [11]:

$$U_\mathrm{s} = 6.72\sqrt{pd} + 24.36(pd)[\mathrm{kV}], \qquad (4)$$

when the pressure times distance, pd, is in the range 10^{-2} to $5{\cdot}10^2$ (bar cm).

In the case of dielectric response, the frequency dependence of the permittivity of the solids, ε^*, needs to be included. Here, the empirical Cole-Cole model [12] is used,

$$\varepsilon^* = \varepsilon(\infty) + \frac{\varepsilon(DC) - \varepsilon(\infty)}{1 + (j\omega\tau)^{1-\alpha}}, \qquad (5)$$

where $\varepsilon(\infty)$ is the permittivity at very high frequencies, $\varepsilon(DC)$ the permittivity at very low frequencies, ω the angular frequency, and τ the temperature-dependent relaxation time. The shape parameter α describes the broadness of the relaxation peak and has a value between 0 and 1. Equation (5) is temperature-dependent according to an Arrhenius relation [13] such that $\tau(T) = \tau_0 \cdot \exp\frac{E_\mathrm{a}}{k_B T}$, where E_a is the activation energy, k_B the Boltzmann constant, and T the temperature in Kelvin.

The capacitive Model 1 is valid at high frequencies when the resistive contribution is low. Model 2 applies at low frequencies when the resistive contribution is higher or comparable to the capacitive contribution, as can be seen in Equation (2) for Model 2. The cut-off frequency f_c between high and low frequencies is described by the Maxwell-Wagner effect for interfacial polarisation between two materials:

$$f_\mathrm{c} = \frac{d_\mathrm{c}\sigma_\mathrm{b} + d_\mathrm{b}\sigma_\mathrm{c}}{d_\mathrm{c}\varepsilon_0\varepsilon_{r,b} + d_\mathrm{b}\varepsilon_0\varepsilon_{\mathrm{r,c}}}. \qquad (6)$$

The inclusion of dielectric response in Model 3 complicates the calculation of the cut-off frequency f_c. As ε_b^* is frequency-dependent, a numerical approach is needed. This can be done by creating a frequency-dependent

estimator $\hat{f}_c$ for f_c in Equation (6) and comparing it to the frequency at the different values for ε_b^*. The cut-off frequency f_c is then defined when $\hat{f}_c = f$.

The void resistance is usually neglected, as the air conductivity is low. The conductivity of air strongly depends on atmospheric conditions and is in the range 10^{-16} to 10^{-13} S/m [14]. The value is drastically reduced if the gas ions are neutralised. This conductivity range corresponds to cut-off frequencies in the range $5 \cdot 10^{-6}$ to $5 \cdot 10^{-3}$ Hz.

PDs produce chemical by-products when in contact with the surrounding gas or dielectric surface. Hudon *et al* [15] determined that PDs react with air and the epoxy surface and create oxidic, formic, glycolic, glyoxylic, and nitric acids, which result in a significantly increased surface conductivity. Test objects are often preconditioned, and during this period such components are likely to be produced, thereby decreasing the void resistivity. This can partly or completely short-circuit voids, significantly increasing the cut-off frequency, while the void models cannot neglect the void resistivity.

The effect of such preconditioning disappears with time [16]. Generally, at elevated temperatures, the PD by-products diffuse or are neutralised faster than they are produced. The temperature dependence is especially large for the self-decomposition of nitric acid [17], which reduces the acidity at higher temperatures and thereby the surface conductivity. Consequently, the decomposition of nitric acid is almost instantaneous at 90°C. Possible effects of PD by-products caused by the preconditioning are, therefore, expected to be active at low temperatures only.

3 EXPERIMENTAL METHODS

3.1 TEST OBJECTS

Square samples with dimensions 100x100x3 mm^3 were produced from a resin-rich mica tape commonly used as the main insulation of bars and coils of motor and hydro and turbo generators with 45% mica, 43% epoxy resin and 12% glass fibre, by weight percent. The samples were cured at 160°C for one hour before being rapidly cooled to 20°C for 5 minutes. Three different test objects with embedded voids were used, as shown in Figure 2. Test object 1 consisted of two layers pressed together, where the void was created in the lower layer by using a thin metal disk during the casting process. This created voids with a smooth surface. The void diameter D was in the range of 3-20 mm and the void gap distance d_c in the range of 0.1-1 mm. Test object 2 consisted of three layers with a drilled hole in the middle layer with a void diameter of 80 mm, much larger than the electrode, giving no electrically stressed sidewalls and a void gap distance of 1 mm. Test object 3 was similar to Test object 2, but with a void diameter of 10 mm and a void gap distance of 0.8 mm. The top and bottom of the cylindrical void in Test object 3 were covered with copper tape, which was connected to the outside of the sample with a thin copper wire. The test objects were clamped between two electrodes with a diameter of 30 mm with the side walls embedded in epoxy and covered with a thin silicon grease layer to prevent any unintended air discharges.

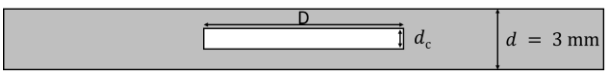

Figure 2. Schematic drawing of the cross section of the test objects.

3.2 MATERIAL CHARACTERISTICS

The insulation material was characterised by dielectric spectroscopy in both time and frequency domain. This can measure the frequency-dependent complex permittivity and DC conductivity, which are important parameters to the presented void voltage models.

The time domain dielectric response tests on the mica/epoxy insulation were performed using 1-mm-thick objects without voids. Aluminium electrodes with a diameter of 40 mm with guard were evaporated to the surface. These samples fitted into an automated measurement setup, as described in [18]. A constant DC voltage in the range of 1 to 8 kV was used. The temperature was set to 40°, 60° and 90°C, in increasing order. The DC voltage was applied for 2 h to measure the polarisation current before the object was grounded for 20 h during depolarisation current measurements.

Dielectric response in the frequency domain was performed on 1 mm thick mica/epoxy samples without voids, by standard methods with IDAX 206 hardware and software. This was done at frequencies in the range of 10^3 to 10^{-4} Hz at 200 V_{peak}. The temperatures were in the range of 20° to 155°C and larger than for the time domain measurements due to limitations of the equipment.

The void resistivity was measured before and after preconditioning on Test object 3 by a DC insulation tester by applying 1 kV DC voltage. This was done to establish whether the preconditioning can decrease the void resistivity or not by a direct resistivity measurement method.

3.3 PD MEASUREMENTS

The PDIV is here defined, in accordance with the definition in IEC 60270 [19], as the voltage level that first produces PDs above a threshold value of 100 pC. Each PDIV data point in this article represents the average result of PD measurements for three similar samples.

The standard PD test setup is shown in Figure 3, as described in e.g. IEC 60034-27 [1]. The Test object (with a capacitance of ~20 pF) was in parallel with a coupling capacitance (100 pF). The measure impedance was in series with the coupling capacitance, Omicron CPL 542, and the data processing unit MPD 600. The high voltage was set by a DAQ and amplified by a TREK 20/20B high voltage amplifier in series with a low-pass filter, with a cut-off frequency at 5 kHz.

The voltage source, heat control, and data measurements were fully automated in LabView. The test procedure was based on the standard method in IEC 60034-27 and IEEE 1434 [1, 2]. The standardised procedure at 50 Hz was expanded to a frequency and temperature sweep, to keep the void condition time variation at a minimum during the test.

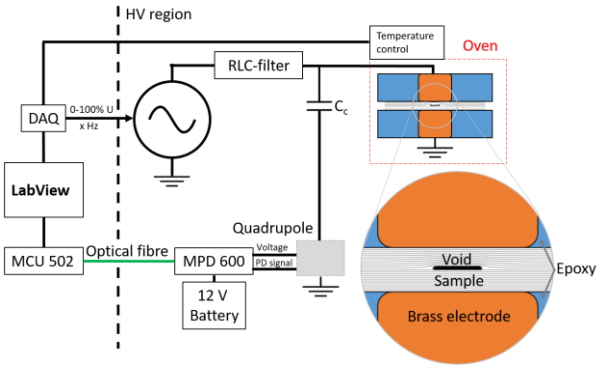

Figure 3. Setup of the PD detection circuit. The setup was controlled by a LabView program.

The procedure of voltage application is shown in Figure 4. It started with a conditioning period of 5 minutes at a maximum test voltage of 10 kV_{RMS} at 50 Hz. Then, the sample was grounded before the voltage was increased in 10 equal steps to maximum test voltage and then decrease in 10 steps back to zero voltage, starting at 300 Hz. The duration of each voltage step was the longest time of 10 s and 10 voltage periods. A minimum of 10 periods was chosen in order to be able to sweep many samples at different frequencies in a limited time. The procedure of voltage application was repeated for several frequencies in decreasing order down to 0.1 Hz. The 50 Hz PDIV test was repeated after the 0.1 Hz PDIV test was finished. The conditioning period at 50 Hz between different frequencies was reduced to 5 s to not influence the void condition but, rather, act as a reference if PDs at 50 Hz changed during the frequency sweep. Both the maximum and total apparent charge during this 5 s period were recorded and used as they can be related to the void voltage [16].

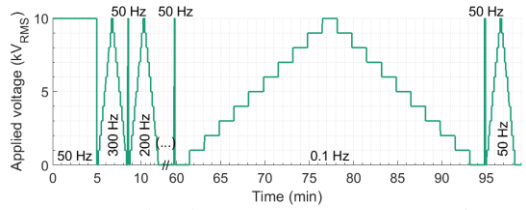

Figure 4. Sketch of the frequency sweep with reducing frequencies.

The temperature was increased in the range of 20° to 155°C after the frequency sweep was finished. A waiting time of 1 hour was shown to be sufficient to reach stable thermal conditions before a new frequency sweep started.

Four samples were tested a second time to check if the frequency and temperature sweep had introduced permanent changes to the samples that influenced the PDIV.

The preconditioning was expected to increase the void conductivity according to Model 2. An increased void conductivity results in a high PDIV. One sample of Test object 1 with a diameter 10 mm and void gap distance 0.5 mm was, therefore, PDIV tested at 0.1 Hz without any preconditioning. This test should indicate whether the preconditioning period increased the value of PDIV at 0.1 Hz.

4 RESULTS AND DISCUSSION

4.1 MATERIAL CHARACTERISATION

The mica/epoxy bulk conductivity was found to be independent of the electric field in the measured range of 1 to 8 kV/mm. It followed an Arrhenius relation with conductivity at 20°C of $\sigma_{20°C} = 5 \cdot 10^{-15}$ S/m and activation energy $E_a = 0.44$ eV with $R^2 = 0.995$.

The void resistance before preconditioning at 20°C was above the instrument limit of 3 TΩ. The void resistance had decreased after the preconditioning to 1 TΩ (corresponding to a void conductivity of $\sigma_c \approx 10^{-11}$ S/m), which means that PD-activity was reducing the void resistance.

The measured values of the real and imaginary parts of the complex permittivity for the tested insulation are given in Figure 5 as data points. The extrapolated conductivity based on the measured values is given as dotted, straight lines. The solid lines correspond to one Cole-Cole mechanism, including the DC conductivity, as described in the temperature-dependent version of Equation (5). The Cole-Cole parameters were curve-fitted to be $\varepsilon(\infty) = 4.42$, $\varepsilon(DC) = 940$, $\tau_0 = 7.4 \cdot 10^{-9} s$, $E_{a,\tau} = 1.00$ and $\alpha = 0.42$. At frequencies above 0.1 Hz, the contribution to dielectric loss from DC conductivity is more than two orders of magnitudes lower than the other losses and can be omitted.

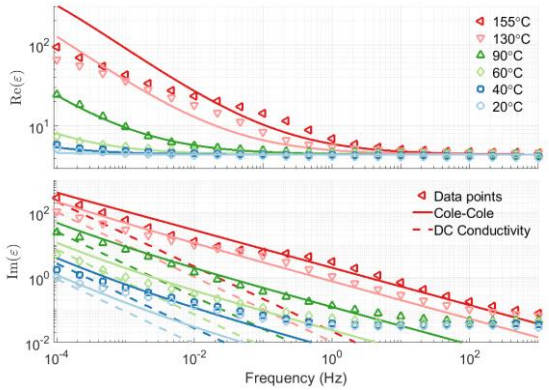

Figure 5. Complex permittivity of the epoxy/mica insulation as a function of frequency for increasing temperatures fitted to a temperature dependent Cole-Cole mechanism and the curve fitted DC-conductivity based on measured dielectric response in the time domain.

4.2 VALIDITY REGIONS OF THE MODELS

A typical insulation system in this study has a void gap distance of 0.5 mm and a mica/epoxy thickness of 2.5 mm. Measured material parameters, together with the assumption of a non-conducting void, have been inserted into the different models. The resulting regions in the temperature-frequency domain, where the different models work, are given in Figure 6. The estimated PDIV cut-off frequencies based on Equation (6) are also included in the figure. All models are equal in the red region (Models 1, 2, 3) where the DC conductivity or dielectric response do not contribute. The conductivity is dominant in the blue region, and Models 2 and 3 are equal. Similarly, in the green region, the dielectric response is dominant, and Model 3 is the only model describing this. The borders between the different regions are

defined as the frequency at which the different models differ more than 5% from each other, and the valid model is assumed to be the most advanced. The limit of 5% was set as a low limit, considering the uncertainties when measuring PDIV in the laboratory and voltage step size. The polarisation losses and insulation conductivity can be neglected above their respective cut-off frequencies, f_c, which is practically always when testing above 0.1 Hz and below 110°C.

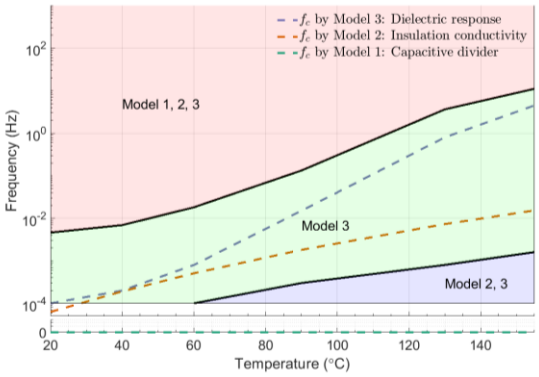

Figure 6. 'Model phase diagram' based on measured values for insulation conductivity and dielectric response for the three different models. The conductivity in the void is assumed to be zero. The estimated Maxwell-Wagener frequency, f_c, is indicated by coloured dotted lines.

4.3 INFLUENCE ON PDIV FROM PRECONDITIONING

A PDIV test at 0.1 Hz without preconditioning on Test object 1 with a diameter 10 mm and a height 0.5 mm demonstrated a PDIV of 5 kV, estimating a low void conductivity. This indicates that the high PDIV at low frequencies after preconditioning - as seen for example in Figure 8 - is a result of the preconditioning period.

A second PDIV test succeeding the first complete frequency and temperature sweep did not produce any significant changes to the PDIV curves. Possible permanent surface changes due to the temperature and electric stress during the test do not seem to affect the PDIV. This means that any increase in conductivity was caused by temporary effects, such as PD by-products that disappeared when the temperature was increased.

The preconditioning was found to influence the void conditions. The total apparent charge during the 5 s conditioning between the different frequencies generally increased with time. This indicated that the preconditioning effect faded with time, similarly to what was seen in [16]. This means that the effect of preconditioning was weaker at lower frequencies than at higher frequencies due to the frequency test order. However, as is seen in the following figures and discussion, the effect remains strong enough to increase the PDIV at low frequencies and thereby predict a reasonable void conductivity. The measured PDIV can be lower than expected if the preconditioning effect fades, resulting in an underestimated void conductivity.

4.4 THE EFFECT OF PRECONDITIONED ELECTRICALLY STRESSED SIDE WALLS

The measured PDIV as a function of frequency for selected sample geometries is given in Figures 7-10. The solid lines represent curve fitting by varying the void conductivity to the dielectric response-based Model 3 in Equation (3). Model 2 could have been used to give equally good estimates to explain trends, but with a minor deviation at high temperatures where the dielectric response is dominating. It was, therefore, considered easier to use Model 3 to fit all the data. Figure 8 describes Test object 1 with a large void diameter (20 mm) and gap distance (0.5 mm) acting as an example for large voids. PDIVs as a function of frequency are all similar for Test object 1 with diameters larger than 10 mm or the gap distance is larger than 0.5 mm.

Test object 2 without electrically stressed sidewalls in Figure 7b has, as expected, zero void conductivity compared to the case in Figure 6. Voids without electrically stressed walls appear as non-conducting. The difference in PDIV at low temperature between Test object 2 in Figure 7 and the other three figures with Test object 1 illustrates that the electrically stressed sidewalls in Test object 1 are important and increases the void conductivity. PD by-products must then deposit at the void sidewall and thereby increase the void conductivity.

The void with a small gap distance (0.1 mm) in Figure 9 shows a smaller frequency dependence than the voids with larger gap distances. The measured low PDIV at low temperatures in a larger frequency range indicates that the void conductivity is lower than for larger gap distances. This indicates that narrow void gaps are less influenced by the PD by-products from the preconditioning than the larger gaps are.

In the case of a small void diameter (3 mm) in Figure 10, measured values of PDIV did not fit the suggested models by being less frequency-dependent than expected. This indicates that the fundamental model assumptions did not hold for void diameters lower than 5 mm. One possible explanation is that the effect of the preconditioning had become weakened and influenced the measured PDIV. The stronger influence at higher temperatures can be due to different time dynamics of the PD by-products due to void geometry.

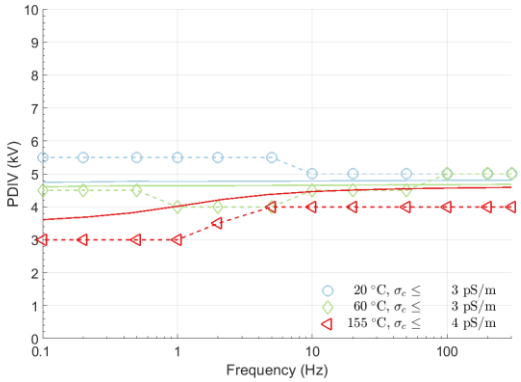

a) PDIV with fitted curves based on Model 3. Markers are measured values, whereas solid lines in the same color represent the theoretical values. $\sigma_c \leq 3$ pS/m, which were the limit by using minimum 0.1 Hz.

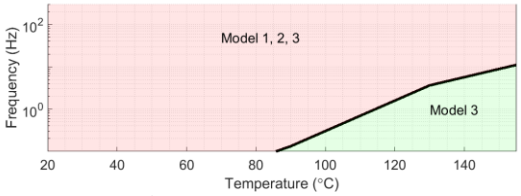

b) Validity regions of presented PDIV models.

Figure 7. PDIV vs frequency for different temperatures for Test object 2, without void walls, with void gap distance 1 mm.

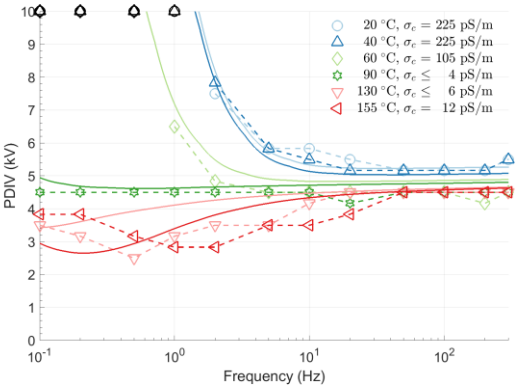

a) PDIV with fitted curves based on Model 3. Markers are measured values, whereas solid lines in the same color represent the theoretical values. Black markers indicate PDIV values higher than 10 kV.

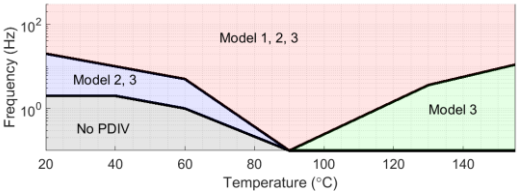

b) Validity regions of presented PDIV models.

Figure 9. PDIV vs frequency for different temperatures for Test object 1, with void diameter 10 mm and gap distance 0.1 mm.

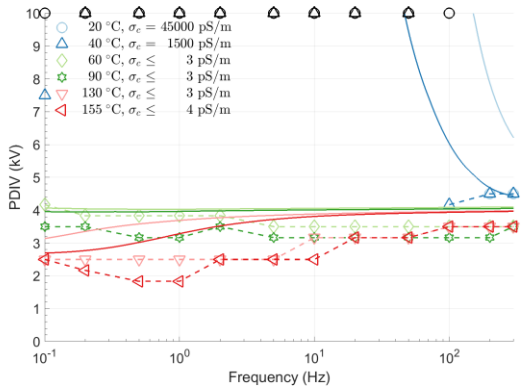

a) PDIV with fitted curves based on Model 3. Markers are measured values, whereas solid lines in the same color represent the theoretical values. Black markers indicate PDIV values higher than 10 kV.

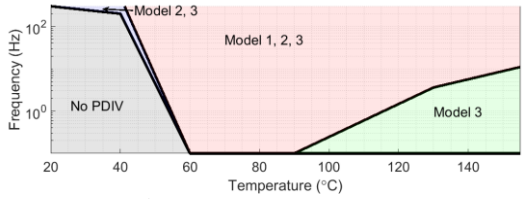

b) Validity regions of presented PDIV models.

Figure 8. PDIV vs frequency for different temperatures for Test object 1, with void diameter 20 mm and gap distance 0.5 mm.

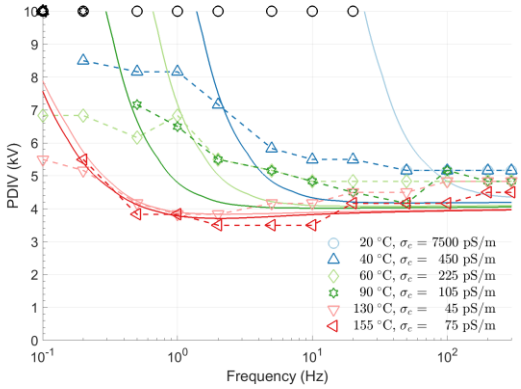

a) PDIV with fitted curves based on Model 3. Markers are measured values, whereas solid lines in the same color represent the theoretical values. Black markers indicate PDIV values higher than 10 kV.

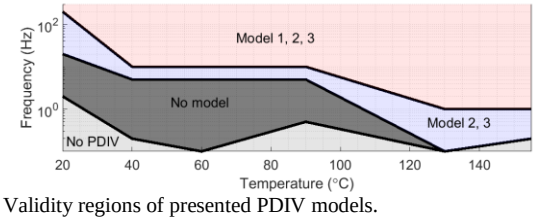

b) Validity regions of presented PDIV models.

Figure 10. PDIV vs frequency for different temperatures for Test object 1, with void diameter 3 mm and gap distance 0.5 mm.

4.5 TEMPERATURE DEPENDENCE OF CALCULATED VOID CONDUCTIVITY

The calculated void conductivities from Model 3 for selected void geometries as a function of temperature are shown in Figure 11. The Arrhenius relation of the void conductivity shows decreasing values with temperature. This is the opposite of what is usually measured for insulation materials where the conductivity increases with temperature. PD by-products deposited at the surface and contributing to the void conductive are, therefore, most likely responsible for this temperature dependence. The involved conductivity processes are not following simple theory, but rather a complex process in which the conductive species are created and assumed to disappear with time and faster at higher temperatures. This can explain the high conductivity at low temperatures and why the conductivity is low at high temperatures, but it needs to be investigated in detail in other studies.

The objects with the smallest void diameters and void gap distances had a different void conductivity temperature dependence than the objects with larger voids. The conductivity remained high, which might indicate that by-products in smaller voids do not relax as fast as in larger voids. This might indicate that the void volume is important for by-product relaxation.

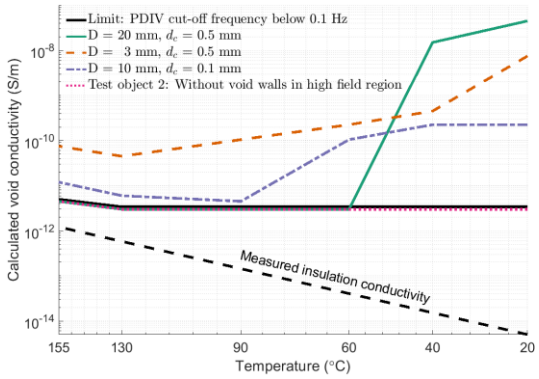

Figure 11. Calculated void conductivity from Model 3 for varying void geometry.

4.6 SIMPLIFIED VOID VOLTAGE MODEL

The mica/epoxy and void air bulk conductivity were demonstrated to be low, resulting in a cut-off frequency below 0.01 Hz. This means that the capacitive Model 1 is sufficient to describe the frequency dependence of PDIV. The capacitive Model 1 must be modified to include the dielectric response at temperatures above 110°C and frequencies above 0.1 Hz. Other limits apply if changing the minimum frequency, according to Figure 6.

The void conductivity can be high and influencing the PDIV when dealing with preconditioned electrically stressed voids at temperatures below 60°C, as was seen by an increased calculated void conductivity in Figure 11. This means that the void conductivity must be included in the model. A simplified version of Model 2 is obtained by expanding Model 1 with the void resistance as presented in Figure 12. The material conductivity was demonstrated to be low and thereby not influencing the PDIV and not included in the model. The simplified Model 2 is valid below 110°C and frequencies above 0.1 Hz, where the permittivity is low and not influencing the PDIV. The model does not fit for voids smaller than 5 mm in diameter. Model 1 can be used if no preconditioning has occurred. The dielectric response must, however, be included if applying frequencies or temperatures outside the limiting values described by Figure 6.

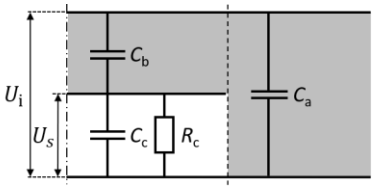

Figure 12. Simplified Model 2, requiring temperatures below 110°C, voltage frequencies above 0.1 Hz and preconditioned voids with diameter larger than 5 mm. The void (wall) resistance R_c can be omitted when no preconditioning has been done or there are no electrically stressed side void walls.

5 CONCLUSIONS

- The frequency-dependent mica/epoxy permittivity was shown to follow the Cole-Cole model. The increased dielectric response at low frequencies at high temperatures decreased the PDIV.
- The calculated void conductivity was dominated by the void surface conductivity.
- PD activity during the preconditioning period at low temperatures increased the void surface conductivity and hence short-circuited the voids at low frequencies resulting in no PDs. This effect was not present at high temperatures. This indicates that the effect of PD by-products decays faster at higher temperatures.
- A simplified model for calculating void voltage that fits well to the measured data is proposed, with two capacitances representing the insulation and the void, and a resistance representing the void wall. This model was a satisfactory approximation for voids with a diameter larger than 5 mm, even though dielectric response had to be included in the model to fit the measured data at temperatures above 110°C.

ACKNOWLEDGMENT

This work is funded by the project 'Hydrogenerator Stator Winding Insulation Assessment'. The project is supported by The Research Council of Norway (Project No. 255099/E20), and industrial partners.

REFERENCES

[1] Off-line partial discharge measurements on the stator winding insulation of rotating electrical machines, IEC TS 60034-27:2006.

[2] IEEE Guide for the Measurement of Partial Discharges in AC Electric Machinery, IEEE Std 1434-2014 (Revision of IEEE Std 1434-2000).

[3] IEEE Recommended Practice for Insulation Testing of AC Electric Machinery with High Voltage at Very Low Frequency, IEEE Std 433-2009 (Revision of IEEE Std 433-1974).

[4] U. Gäfvert, H. Edin and C. Forssén, "Modelling of partial discharge spectra measured with variable applied frequency," *IEEE Int. Conf. Prop. Appl. Dielectr. Mat.(ICPADM)*, 2003, vol. 3, pp. 839-842.
[5] C. Forssen and H. Edin, "Partial discharges in a cavity at variable applied frequency part 1: measurements," IEEE Trans. Dielectr. Electr. Insul., vol. 15, no. 6, pp. 1601-1609, 2008.
[6] C. Forssen and H. Edin, "Partial discharges in a cavity at variable applied frequency part 2: measurements and modeling," IEEE Trans. Dielectr. Electr. Insul., vol. 15, no. 6, pp. 1610-1616, 2008.
[7] H. Illias, G. Chen and P. Lewin, "Partial discharge behavior within a spherical cavity in a solid dielectric material as a function of frequency and amplitude of the applied voltage," IEEE Trans. Dielectr. Electr. Insul., vol. 18, no. 2, pp. 432-443, 2011.
[8] H. A. Illias, G. Chen, and P. L. Lewin, "Partial discharge measurements for spherical cavities within solid dielectric materials under different stress and cavity conditions," *Annu. Rep. Conf. Electr. Insul. Dielectr. Phenom. (CEIDP)*, 2009, pp. 388-391.
[9] G. Callender, T. Tanmaneeprasert, and P. L. Lewin, "Simulating partial discharge activity in a cylindrical void using a model of plasma dynamics," J. Phys. D: Appl. Phys., vol. 52, no. 5, p. 055206, 2019.
[10] M. Lévesque, E. David, and C. Hudon, "Effect of surface conditions on the electric field in air cavities," IEEE Trans. Dielectr. Electr. Insul., vol. 20, no. 1, pp. 71-81, 2013.
[11] E. Kuffel and W. S. Zaengl, *High-voltage engineering: fundamentals*, Pergamon Press, 1984.
[12] K. S. Cole and R. H. Cole, "Dispersion and absorption in dielectrics I. Alternating current characteristics," J. Chem. Phys., vol. 9, no. 4, pp. 341-351, 1941.
[13] K. C. Kao, *Electric Polarization and Relaxation. Dielectric Phenomena in Solids*. San Diego, Academic Press, 2004 p. 99.
[14] M. Saltzer, U. Gäfvert, B. Källstrand, K. Johansson and L. Walfridsson, "Observation of space charge dynamics in air under DC electric fields," *Annu. Rep. Conf. Electr. Insul. Dielectr. Phenom. (CEIDP)*, 2011, pp. 141-144.
[15] C. Hudon, R. Bartnikas and M. R. Wertheimer, "Effect of physico-chemical degradation of epoxy resin on partial discharge behavior," IEEE Trans. Dielectr. Electr. Insul., vol. 2, no. 6, pp. 1083-1094, 1995.
[16] T. G. Aakre, E. Ildstad, and S. Hvidsten, "Time Development of Voltage Frequency Dependence of Partial Discharge Activity in Voids," *Nordic Insul. Symp. (NordIS)*, 2019.
[17] G. D. Robertson, D. M. Mason, and W. H. Corcoran, "The Kinetics of the Thermal Decomposition of Nitric Acid in the Liquid Phase," J. Phys. Chem., vol. 59, no. 8, pp. 683-690, 1955.
[18] T. A. Ve, F. Mauseth, and E. Ildstad, "Effect of water content on the conductivity of XLPE insulation," *Annu. Repo. Conf. Electr. Insul. Dielectr. Phenom. (CEIDP)*, 2012, pp. 649-653.
[19] High-voltage test techniques - Partial discharge measurements, IEC 60270:2000.

Torstein Grav Aakre received the M.Sc degree from the Norwegian University of Technology and Science (NTNU) in Trondheim, Norway in 2013. He was then employed by SINTEF Energy Research. In 2016, he started a Ph.D. at NTNU regarding condition assessment of hydropower generator bars. His research interests are within electrical insulation materials, with a focus on condition assessment, conductivity and breakdown mechanisms.

Erling Ildstad received the M.Sc. degree in technical physics in 1978 and the Ph.D. degree in electrical power engineering in 1982 from NTNU in Trondheim, Norway. He has been a full-time professor of high voltage engineering at NTNU since 1993.

Sverre Hvidsten received the M.Sc. degree in 1992 at the Norwegian Institute of Technology (NTH) in Trondheim. During 1993 - 1994 he was a researcher at EFI in Norway. In 1999 he gained the Ph.D. in electrical engineering at The Norwegian University of Science and Technology (NTNU) in Trondheim. He now works as a Senior Research Scientist at SINTEF Energy Research (SEfAS).